Fluid Phase Equilibria 584 (2024) 114125

Contents lists available at ScienceDirect

Fluid Phase Equilibria

journal homepage: www.sciencedirect.com/journal/fluid-phase-equilibria

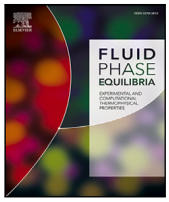

Bulk and interfacial thermodynamics of ammonia, water and their mixtures

Ailo Aasen [a,*], Vegard G. Jervell [b], Morten Hammer [a,b], Bjørn A. Strøm [a], Hans L. Skarsvåg [a], Øivind Wilhelmsen [a,b]

[a] SINTEF Energy Research, Trondheim, NO-7465, Norway
[b] Norwegian University of Science and Technology, Department of Chemistry, Trondheim, NO-7491, Norway

ARTICLE INFO

Keywords:
Ammonia
Water
Equation of state
Density functional theory
Density gradient theory
Surface tension

ABSTRACT

Ammonia is a promising energy carrier for the green transition, but its hygroscopicity and toxicity necessitate in-depth understanding of its interaction with water. This work examines the bulk and interfacial thermodynamics of the ammonia–water system. Parameters for three equations of state are fitted to experimental data and compared to parameters from literature: PC-SAFT, Cubic Plus Association and Peng–Robinson. Peng–Robinson stands out as most accurate for bulk thermodynamics. Introducing a temperature-dependent volume shift for water with Peng–Robinson yields a highly accurate model without introducing problematic inconsistencies, with errors of 0.05% for saturation pressures, and 0.5% for liquid densities. For the mixture, Peng–Robinson with a two-parameter Huron–Vidal mixing rule reproduces measurements mostly within their uncertainties, whereas the standard mixing rules for PC-SAFT and CPA are less accurate. A literature review of surface tension measurements of ammonia–water mixtures reveals that accurate measurements exist only at ambient temperature. We apply density gradient theory and density functional theory based on PC-SAFT, finding that both models fail at reproducing qualitative features of the surface tensions and adsorptions of dilute solutions of aqueous ammonia. Whereas bulk properties are well characterized, understanding and describing the interfacial thermodynamics of the ammonia–water system demands more work both on the experimental and modeling side.

1. Introduction

Ammonia and its mixtures with water feature in numerous applications [1,2], including household cleaning [3], water treatment [4], food production [5], and refrigeration cycles [6]. It is present in parts-per-billion concentrations in the atmosphere, where water, ammonia and sulfuric acid play a key role in aerosol nucleation [7]. In the context of the green transition, ammonia is being evaluated as a potential energy carrier and a sustainable fuel [8,9], especially in the maritime sector [2]. Large-scale adoption would demand a drastic increase in storage capacity, and new use cases may require updates to the otherwise mature safety regulations. Large storage tanks are foreseen to store ammonia in refrigerated form at its boiling point of 239.8 K (−33.3 °C) and atmospheric pressure. Should the maritime industry adopt this fuel, tanks would commonly be situated in harbors and aboard vessels. At sea, a leak of liquid ammonia can mix with seawater, and on land ammonia vapor can mix with humid air, forming a gas with suspended ammonia–water droplets. Understanding the evolution of such a fog requires understanding both the bulk and interfacial thermodynamics of the ammonia–water–air system.

With regards to safety, ammonia toxicity is the main concern. Ammonia is lethal to humans already at small concentrations (5000 parts per million) and short exposure times [10]. For maritime applications, environmental considerations must also be taken into concern. Fish death occurs at minuscule concentrations, with acute toxicity levels in the 2–3 parts per million range [11]. This sensitivity to small concentrations for both safety and environmental applications places stringent demands on the accuracy of thermodynamic sub-models used in ammonia dispersion models. Accurate vapor–liquid equilibrium compositions are crucial for the mass balance, as are enthalpies for the energy balance. Other key requirements of thermodynamic models for dispersion modeling are robustness and low computational cost.

Both ammonia and water are small, polar molecules capable of hydrogen bonding. A physically rigorous approach to model hydrogen bonding was presented by Wertheim [12–15], which is incorporated into cubic plus association (CPA) and statistical associating fluid theory (SAFT)-type equations of state. Several SAFT models that explicitly account for association between the molecules have been fitted for the ammonia–water system, including GC-PPC-SAFT [16], SAFT-VR [17], SAFT-VR Mie [18], CP-PC-SAFT [18], and PC-SAFT [19]. The

* Corresponding author.
E-mail address: ailo.aasen@sintef.no (A. Aasen).

https://doi.org/10.1016/j.fluid.2024.114125
Received 1 March 2024; Received in revised form 7 May 2024; Accepted 7 May 2024
Available online 18 May 2024

association term requires fitting an energy scale parameter and a volume scale parameter to experimental data, but the parameters may in practice also capture other effects such as dipole–dipole interactions. Theories such as PCP-SAFT [20] attempt to explicitly incorporate dipole interactions, but at least for water, this does not seem to offer any clear improvement with respect to PC-SAFT [21]. Finally, we emphasize that these effects do not have to be explicitly modeled; engineering approaches such as the cubic equation of state E-PPR78 [22] can still achieve high accuracy by using advanced mixing rules.

Whereas the bulk thermodynamic properties of the ammonia–water mixture are accurately known, the interfacial properties have been less studied. Even for the planar surface tension, few experimental data sets are available in the open literature [23–25], and the surface tension of the ammonia–water mixture is only known with reasonable accuracy at room temperature. In the modeling of ammonia–water fogs, accurate mass balances are likely to require an adsorption model due to the potentially large surface area of the suspended droplets. Surface tensions and adsorptions cannot be calculated from an equation of state (EoS) alone, since they are interfacial properties. Density gradient theory (DGT) [26,27] and non-local density functional theory (DFT) [28–30] are methods that can calculate these properties. DGT can be combined with any EoS with a single van der Waals loop between the binodals [31], although it is still not fully understood how the EoS behavior impacts predicted interfacial properties.

There are highly accurate multiparameter EoS available for the ammonia–water mixture [32,33], but there are at least three reasons why new parameters are fitted in this work. First, there is an increasing demand for computationally efficient and robust EoS for use in consequence and risk analysis of ammonia spills with computational fluid dynamics (CFD) [34]. Secondly, the vast majority of multiparameter EoS have a second, unphysical van der Waals loop [31], which precludes their use in calculating interfacial properties with DGT or DFT. Moreover, since ammonia will also interact with air there is a need for EoS that can easily be applied to mixtures with a large number of components. The aim of this work is therefore to explore the potential of some of the most promising correlative EoS, namely Peng–Robinson, CPA and PC-SAFT, in representing bulk and interfacial properties of the water–ammonia mixture.

2. Theory

In the following, the EoS used in this work will be described in Section 2.1, and the methods used to calculate interfacial properties will be described in Section 2.2. The ideal contribution to the Helmholtz energy is the same for all EoS, equal to that of the reference EoS described in Section 2.1.5.

2.1. Equations of state

2.1.1. PC-SAFT equation of state

Perturbed Chain Statistical Associating Fluid Theory (PC-SAFT) is a molecular-based equation of state derived from thermodynamic perturbation theory using a hard-chain reference system [35,36]. The molecular model is parameterized by the monomer diameter σ, the chain length m, and the dispersive energy scale ε. If the molecule is capable of hydrogen bonding, two additional parameters appear: an energy scale $\varepsilon^{\text{assoc}}$ and an adimensional volume scale β^{assoc}, corresponding to the strength and the size of a potential well for association. The reduced Helmholtz energy is $a = A/(nRT)$, where A is the total Helmholtz energy, n is the number of moles, R is the gas constant and T is temperature. It can be decomposed into the following contributions

$$a = a^{\text{ig}} + a^{\text{hs}} + a^{\text{hc}} + a^{\text{disp}} + a^{\text{assoc}}, \tag{1}$$

corresponding to ideal gas, hard-sphere, hard-chain, dispersion and association contributions. PC-SAFT represents an equation of state with a foundation in statistical mechanics that has been used extensively for interfacial thermodynamics [21,37,38].

Different parametrizations of the association term are used in the PC-SAFT literature, which necessitates detailing this term. All variants use the Wertheim expression

$$a^{\text{assoc}} = \sum_i z_i \sum_{A_i} \left(\ln X_{A_i} - \frac{X_{A_i}}{2} + \frac{1}{2} \right) \tag{2}$$

where z_i is the mole fraction of component i, and X_{A_i} is the fraction of component-i molecules not bonded at the site A_i. The nonbonded fractions are solved from

$$1/X_{A_i} = 1 + \rho \sum_j z_j \sum_{B_j} X_{B_j} \Delta^{A_i B_j}. \tag{3}$$

Differences arise from how the association strength $\Delta^{A_i B_j}$ between the association sites A_i and B_j is modeled. The PC-SAFT equation of state uses the form

$$\Delta^{A_i B_j} = g_{ij}(d_{ij}) \kappa^{A_i B_j} \sigma_{ij}^3 [\exp(\varepsilon^{A_i B_j}/RT) - 1] \tag{4}$$

where $g_{ij}(d_{ij})$ is a hard-sphere mixture radial distribution function evaluated at the hard sphere diameter d_{ij} for the ij interaction [39,40]. The parameters $\kappa^{A_i B_j}$, σ_{ij} and $\varepsilon^{A_i B_j}$ are binary parameters of the equation of state, which are related to their pure-component parameters according to

$$\sigma_{ij} = \frac{\sigma_i + \sigma_j}{2}$$
$$\kappa^{A_i B_j} = \sqrt{\kappa^{A_i B_i} \kappa^{A_j B_j}} \left(\sqrt{\sigma_i \sigma_j}/\sigma_{ij} \right)^3$$
$$\varepsilon^{A_i B_j} = \frac{\varepsilon^{A_i B_i} + \varepsilon^{A_j B_j}}{2}$$

NguyenHuynh et al. [19] have not stated the formulation they use for a^{assoc} explicitly, but to reproduce results from their model we had to apply the hard sphere diameter $d(T)$ in place of the segment diameter σ_{ij} in Eq. (4). Gross and Sadowski, on the other hand, use the form in Eq. (4) [36]. Various mixing rules for PC-SAFT have been proposed over the years; we used the original mixing rules that were applied by Gross and Sadowski [35,41,42].

2.1.2. SAFT-VR Mie equation of state

Statistical associating fluid theory for variable range interactions of the generic Mie form (SAFT-VR Mie) is a molecular-based equation of state derived from thermodynamic perturbation theory based on a hard-sphere reference system [43]. The reduced Helmholtz energy can also be written in the form Eq. (1), although the terms are treated differently. Notably, the monomer interaction is assumed to be described by a Mie potential. We used the association term based on the generic Mie kernel defined by Dufal et al. [44].

In this work we do not fit any new data sets for SAFT-VR Mie, but we evaluate the literature models for ammonia and water [44].

2.1.3. Peng-Robinson equation of state

The Peng–Robinson (PR) EoS [45,46] is a cubic EoS that can be written in pressure-explicit form as

$$P = \frac{RT}{v - b} - \frac{a}{(v - r_1 b)(v - r_2 b)}, \tag{5}$$

where v is the molar volume, R is the gas constant, $\boldsymbol{z}$ are the mole fractions, $a = a(T, \boldsymbol{z})$ is the attraction parameter, $b = b(\boldsymbol{z})$ is the covolume, and $(r_1, r_2) = (-1 - \sqrt{2}, -1 + \sqrt{2})$. For a pure component, the parameters a and b are

$$a(T) = a_0(T_c, P_c)\alpha(T) \tag{6}$$

$$b = b_0(T_c, P_c) \tag{7}$$

where a_0, b_0 are functions that ensure that the experimental critical temperature T_c and pressure P_c are exactly reproduced by the EoS. We used the alpha function by Twu et al. [47],

$$\alpha(T) = (T/T_c)^{N(M-1)} \exp[L(1 - (T/T_c)^{MN})], \tag{8}$$

Table 1
Triple point temperature T_t and critical temperature, pressure and density. Pure ammonia values are from Ref. [1] and water values from Ref. [55].

	T_t (K)	T_c (K)	P_c (bar)	ρ_c ($\frac{\text{mol}}{\text{m}^3}$)
Ammonia	195.49	405.56	113.63	13 696
Water	273.16	647.096	220.64	17 873.7

due to its versatility.

Mixing rules. To calculate a and b for mixtures we used the Huron–Vidal mixing rule [48]:

$$\frac{a(T,\boldsymbol{z})}{b(\boldsymbol{z})} = \sum_i z_i \frac{a_i(T)}{b_i} - \frac{a_\infty^{\mathrm{E},\gamma}(T,\boldsymbol{z})}{h_\infty}. \tag{9}$$

$$b(\boldsymbol{z}) = \sum_i z_i b_i. \tag{10}$$

Here a_i, b_i are the pure-component parameters, and $h_\infty = \frac{1}{r_2 - r_1} \ln \frac{1-r_1}{1-r_2} = \log(\sqrt{2}+1)/\sqrt{2}$. The molar excess Helmholtz energy, $a_\infty^{\mathrm{E},\gamma}$, is given by a modified non-random two-liquid (NRTL) model:

$$\frac{a_\infty^{\mathrm{E},\gamma}}{RT} = \sum_i x_i \frac{\sum_j \tau_{ji} b_j x_j \exp(-\alpha_{ji}\tau_{ji})}{\sum_k b_k x_k \exp(-\alpha_{ki}\tau_{ki})}, \quad \tau_{ji} = \frac{\Delta g_{ji}}{RT}. \tag{11}$$

Moreover, $\Delta g_{ii} = 0$. In this work we set $\alpha_{ij} = \alpha_{ji} = 0.03$. Δg_{ji} is assumed to be independent of temperature. The Huron–Vidal mixing rule thus requires fitting the two parameters Δg_{12} and Δg_{21} to experimental data for the mixture.

Volume shift. Cubic equations of state generally mispredict liquid densities, but this can be remedied with a volume shift [49,50]. The volume-shifted EoS is obtained by the translation $v \to v + c$:

$$P = \frac{RT}{v + c - b} - \frac{a}{(v + c - r_1 b)(v + c - r_2 b)}, \tag{12}$$

The quantity $b - c$ is referred to as the effective covolume [50], and c is usually on the order of a few percent of b. A volume shift thus has negligible impact at low densities, but potentially a large impact for dense phases. A temperature-independent volume shift does not affect saturation pressures, latent heats, or heat capacities [50]. In this work we have also tested a linear temperature dependence for the volume shift of pure fluids,

$$c(T) = \epsilon_0 + \epsilon_1 T. \tag{13}$$

Temperature-dependent volume-shifts will lead to negative isochoric heat capacities at sufficiently high pressures [51]. For quantum fluids it was recently shown [52] that such unphysicalities can be made to occur only at extreme pressure or temperature, and thus offer no practical problem. We will show that this is also the case for water.

For a mixture, the linear mixing rule

$$c(\boldsymbol{z}) = \sum_i z_i c_i, \tag{14}$$

is applied, and can be shown to not affect predicted VLE compositions [53]. A temperature-dependence in the pure-component shifts c_i will thus carry over to the mixture shift c.

Values of critical parameters. Since cubic EoS are designed to reproduce the critical temperature T_c and pressure P_c, these in effect become parameters of the EoS. The critical point estimates are ever-evolving, and hence different EoS implementations use different values. In this work we have used the Thermopack values [31,54]: $T_c = 647.3$ K, $P_c = 220.483$ bar for water, $T_c = 405.6$ K, $P_c = 114.7$ bar for ammonia. These differ by less than 0.1% from the current reference values given in Table 1, except for P_c for ammonia which differs by 1%.

2.1.4. Cubic plus association equation of state

The Cubic Plus Association (CPA) EoS was developed by Kontogeorgis et al. [56] by adding the Wertheim association term to the SRK cubic EoS [57]. SRK is represented by Eq. (5) with $r_1 = 0$ and $r_2 = -1$. This work uses the CPA-SRK model with the simplified mixing rules described in Kontogeorgis et al. [58]. The parameters for water were taken from Ref. [59], while the parameters for ammonia were fitted.

The binary parameter we fitted for CPA-SRK is k_{ij} in the conventional mixing rule of the SRK EoS:

$$a(T,\boldsymbol{z}) = \sum_i \sum_j z_i z_j (a_i a_j)^{1/2}(1 - k_{ij}) \tag{15}$$

$$b(\boldsymbol{z}) = \sum_i z_i b_i \tag{16}$$

For the association strength we used the Elliot combining rule:

$$\Delta_{ij} = (\Delta_{ii}\Delta_{jj})^{1/2}, \tag{17}$$

which introduces no interaction parameters.

Since CPA uses the critical temperature in its correlation of the alpha function, one must ensure to use the value that is consistent with the other parameters. The CPA parameters fitted in this work have used the Thermopack values.

2.1.5. Reference, multiparameter equations of state

Highly accurate reference equations of state for pure ammonia [1] and pure water [55] exist, which mostly reproduce experimental data within their uncertainty. Results from these reference EoS have been used to fit the other equations of state. The water reference EoS has uncertainties on the order of 0.05% in vapor pressure, while for saturated liquid it is 0.01% in density, 0.1% in isobaric heat capacity, and 0.5% in isochoric heat capacity. The ammonia reference EoS indicates uncertainties of 0.1% in vapor pressure and 0.1% for saturated liquid density; for heat capacities the uncertainty is unclear, but 2% seems to be a conservative estimate for the isobaric and isochoric heat capacities for saturated liquids.

The bulk thermodynamic properties of ammonia–water mixtures are also accurately known. Already in 1998 the reference equation of state by Tillner-Roth and Friend [33] was able to reproduce experimental measurements of density to within ±0.3% (relative), enthalpies within ±200 J/mol (absolute), and vapor–liquid mole fractions with uncertainty ±0.01 (absolute). The REFPROP 10 software includes an even more accurate (unpublished) EoS [32], which we used for fitting binary interaction parameters for the simpler equations of state.

2.2. Interfacial thermodynamics

To describe interfacial properties, we introduce a *dividing surface* [60], which makes the liquid volume V^ℓ and the vapor volume V^g well-defined. Calculations then proceed in terms of excess quantities relative to this (arbitrarily positioned) surface, which are usually normalized by the surface area A_s. Key interfacial properties are the surface tension and the adsorptions:

$$\sigma = \frac{\Omega - \omega^\ell V^\ell - \omega^\mathrm{g} V^\mathrm{g}}{A_s} \qquad \text{(surface tension)}, \tag{18}$$

$$\boldsymbol{\Gamma} = \frac{\boldsymbol{N} - \boldsymbol{\rho}^\ell V^\ell - \boldsymbol{\rho}^\mathrm{g} V^\mathrm{g}}{A_s} \qquad \text{(adsorptions)}. \tag{19}$$

The surface tension is the excess grand free energy per area, where Ω is grand free energy of the system and ω is the grand free energy density. The adsorptions $\boldsymbol{\Gamma}$ contain the excess number of particles per surface area A_s. Here $\boldsymbol{\rho}$ is the vector of concentrations in the bulk liquid (superscript ℓ) and the bulk vapor (superscript g), while $\boldsymbol{N}$ is the total number of particles of each component in the system.

The Gibbs adsorption equation [60] links these interfacial properties along an isotherm:

$$\mathrm{d}\sigma = -\boldsymbol{\Gamma} \cdot \mathrm{d}\boldsymbol{\mu} + \left(\frac{\partial \sigma}{\partial r}\right)_{T,\boldsymbol{\mu}} \mathrm{d}r. \tag{20}$$

where r is the location of the dividing surface. The last differential captures the effect of moving the dividing surface without any physical

changes to the system, i.e. with temperature and chemical potentials held constant. We only consider planar interfaces, for which this latter quantity is zero.

In this work we have used the total equimolar surface, defined as $\sum_i \Gamma_i = 0$. If the surface tension is measured along an isotherm and correlated in terms of a parameter x_1, and an accurate equation of state [32] is used to calculate chemical potentials along the VLE locus, the Gibbs adsorption equation can be used to calculate the adsorptions:

$$\left.\frac{\partial \sigma}{\partial x_1}\right|_T = -\boldsymbol{\Gamma} \cdot \left.\frac{\partial \boldsymbol{\mu}}{\partial x_1}\right|_T . \tag{21}$$

Here x_1 can be any convenient variable, which in this work was chosen to be the liquid mole fraction of ammonia. Together with the condition $\sum_i \Gamma_i = 0$ this allows the adsorptions $\boldsymbol{\Gamma}$ to be determined.

2.2.1. Density functional theory

The thermodynamic properties of the gas–liquid interface can be computed using classical density functional theory (DFT), in which the grand potential of the system is expressed as a functional of the density profiles of each component,

$$\Omega[\boldsymbol{\rho}] = A[\boldsymbol{\rho}] + \int \boldsymbol{\rho}(\boldsymbol{r}) \cdot (\boldsymbol{V}_{\text{ext}}(\boldsymbol{r}) - \boldsymbol{\mu}) \mathrm{d}\boldsymbol{r} \tag{22}$$

where A denotes the total Helmholtz energy and $\boldsymbol{V}_{\text{ext}}$ denotes the external potential experienced by each species, set to zero in this work. The Helmholtz energy functional is expressed as

$$A[\boldsymbol{\rho}] = k_B T \int \phi(\boldsymbol{r}) \mathrm{d}\boldsymbol{r}, \tag{23}$$

where ϕ is the reduced Helmholtz energy density. The equilibrium density profiles are found by minimizing the grand potential of the system, by solving the equations

$$\frac{\delta A[\boldsymbol{\rho}]}{\delta \rho_i(\boldsymbol{r})} = \mu_i^b, \tag{24}$$

where μ_i^b denotes the chemical potential in the bulk phases. The reduced Helmholtz energy density we use is based on the PC-SAFT equation of state and is given as

$$\phi = \phi^{\text{id}} + \phi^{\text{hs}} + \phi^{\text{hc}} + \phi^{\text{disp}} + \phi^{\text{assoc}}. \tag{25}$$

Here each contribution is, in general, a function of a set of weighted densities,

$$\phi^\alpha = \phi^\alpha(\boldsymbol{n}), \quad n_i = \sum_j w_j^{(i)} * \rho_j, \tag{26}$$

with $*$ denoting a convolution, and $w_j^{(i)}$ denoting various weight functions. For details, the reader is referred to the supplementary material and Refs. [61–65].

In practice, Eq. (24) is solved by iterating the set of equations

$$\rho_i(\boldsymbol{r}) = \frac{N \Lambda_i^{-3} \exp\left[\beta\left(\mu_i - \frac{\delta A}{\delta \rho_i}\right)\right]}{\sum_j \Lambda_j^{-3} \int \exp\left[\beta\left(\mu_j - \frac{\delta A}{\delta \rho_j}\right)\right] \mathrm{d}\boldsymbol{r}}, \quad i \in \{\mathrm{H_2O}, \mathrm{NH_3}\} \tag{27}$$

where Λ_i is the de Broglie wavelength of species i, N is a specified total number of molecules in a control volume containing the interface, and μ_i are the chemical potentials computed at the bulk conditions, using a damped fixpoint iteration [65].

For this work, we adopt the White Bear fundamental measure theory functional [62,66] for the hard sphere contribution (ϕ^{hs}), the hard-chain (ϕ^{hc}) and dispersion (ϕ^{disp}) contributions due to Sauer and Gross [61], and the association contribution (ϕ^{assoc}) from Yu and Wu [67]. Further details are included in the supplementary material.

2.2.2. Density gradient theory

As an alternative to DFT one can use density gradient theory (DGT) [60,68]. In DGT, the Helmholtz energy functional is

$$A[\boldsymbol{\rho}] = \int \left(a^{\text{EOS}}(\boldsymbol{\rho}) + \frac{1}{2}\sum_{ij} \kappa_{ij} \boldsymbol{\nabla}\rho_i \cdot \boldsymbol{\nabla}\rho_j\right) \mathrm{d}\boldsymbol{r}. \tag{28}$$

Here κ_{ij} are the entries of a symmetric and positive semidefinite matrix known as the *influence matrix*, and $a^{\text{EOS}}(\boldsymbol{\rho})$ is the Helmholtz energy density of a fluid with uniform densities $\boldsymbol{\rho}$ at the specified temperature. The Helmholtz energy density a^{EOS} is modeled with an EoS, where $a^{\text{EOS}}(\boldsymbol{\rho}) = -P^{\text{EOS}}(\boldsymbol{\rho}) + \boldsymbol{\mu}^{\text{EOS}}(\boldsymbol{\rho}) \cdot \boldsymbol{\rho}$. For a pure component i the influence matrix is a scalar κ_i, which is fitted to the planar surface tension of the component. For mixtures we used the combining rule

$$\kappa_{ij} = (1 - \beta_{ij})\sqrt{\kappa_i \kappa_j} \tag{29}$$

which reduces to the geometric combining rule when $\beta_{ij} = 0$.

A key difference between DFT and DGT is that the former is a predictive approach, whereas the influence matrix of DGT is tuned at each temperature. When modeling a binary mixture such as ammonia–water, DGT has three temperature-dependent parameters.

3. Model regression

For information on which parameters that have been fitted for each model, we refer to Section 2. This section describes the methodology that has been used in the regression.

3.1. Regression of EoS parameters for pure fluids

For ammonia, the properties were fitted between the triple point and $0.9T_c$. For water, we fitted vapor–liquid saturation properties between 250 K and 518 K, where the latter corresponds to $0.8T_c$. Below the triple point temperature of 273.16 K, the vapor–liquid equilibrium is metastable with respect to ice formation. This metastable temperature range is included in the fitting process since ammonia–water fluid mixtures can be stable at such temperatures, which means that water must still be reasonably described by the EoS. The metastable properties were calculated from the IAPWS equation of state [55], which is highly accurate down to 250 K [69].

The parameters $\boldsymbol{\Lambda}$ of an EoS were fitted by solving the minimization problem

$$\min_{\boldsymbol{\Lambda}} \left(\sum_{i=1}^{50} \sum_{X_i} w(X_i) \times \left| \frac{X_i^{\text{EoS}}(\boldsymbol{\Lambda}) - X_i^{\text{ref}}}{X_i^{\text{ref}}} \right| \right), \tag{30}$$

where for each saturation state i, X_i ranged over the following properties: pressure p^{sat}, liquid density $\rho^{\text{sat}}(\ell)$, latent heat Δh^{sat}, liquid isochoric heat capacity $c_v^{\text{sat}}(\ell)$, and liquid isobaric heat capacity $c_p^{\text{sat}}(\ell)$. The weight $w(X)$ was set to 1 for pressure and 0.1 for all other properties. The properties X^{ref} were calculated from the reference EoS for ammonia [1] or water [55]. The 50 states were equispaced in temperature, with initial and final temperature as specified above.

Since we are fitting temperature-dependent covolumes, and since these affect heat capacities [50], it is crucial to incorporate heat capacities in the objective function.

The reason why vapor pressure deviations are penalized ten times as much as the other properties is that it is a prerequisite for accurate correlation of Pxy VLE behavior. Additionally, the Clausius–Clapeyron relation $dp^{\text{sat}}/dT = \Delta h^{\text{sat}}/(T\Delta v^{\text{sat}})$ connects the vapor pressure with both the enthalpy h and volume v of phase change where superscript sat refers to saturation properties. To prevent errors in Δh^{sat} and Δv^{sat} from conspiring to yield an accurate $dp^{\text{sat}}(T)/dT$, we also include Δh^{sat} in the objective function.

3.2. Regression of EoS for binary mixtures

We used the reference EoS for the binary mixture from REFPROP 10 [32]. The EoS were fitted to vapor–liquid equilibrium mole fractions

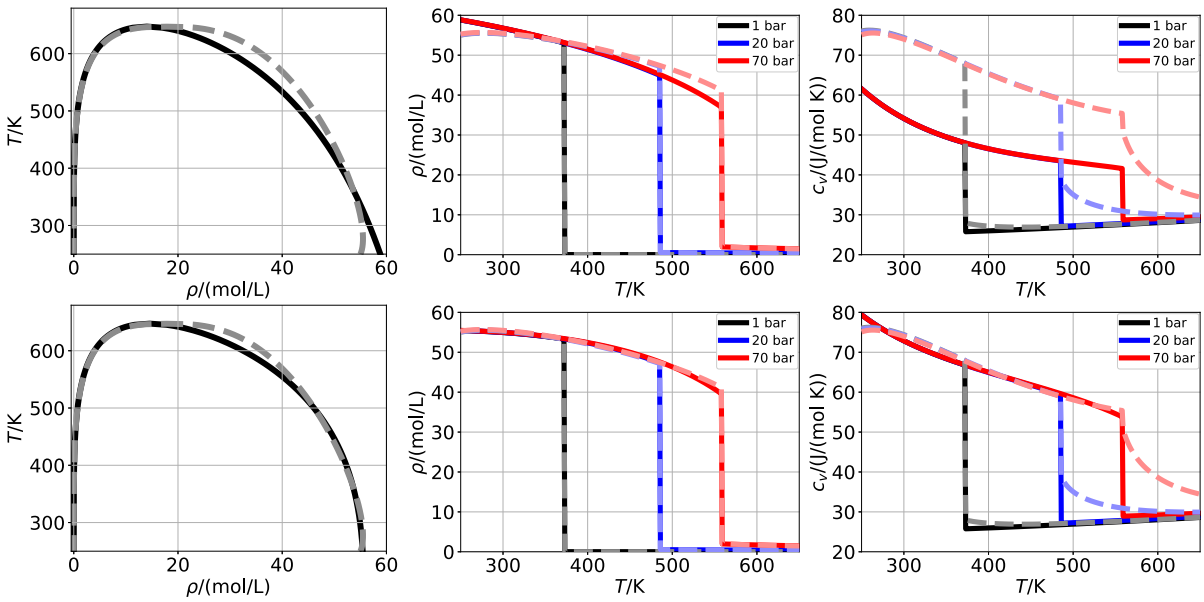

Fig. 1. Results for water for the PR EoS with constant volume shift (top row) and with volume shift linear in temperature (bottom row). Left column: saturation densities. Center column: density isobars. Right column: isochoric heat capacities. Full lines are the fitted EoS, while dashed lines represent the reference EoS.

at temperatures 250 K, 273.15 K, 300 K, 350 K, 400 K, and 450 K. Although not fitted, the performance of the EoS for enthalpic and volumetric properties are also evaluated in Section 4.

3.3. Regression of parameters in density gradient theory

Density gradient theory uses a temperature-dependent influence parameter. It was fitted so as to exactly reproduce the single-component surface tension correlations by Mulero et al. [70]. For binary mixtures we fitted the β_{ij} parameter, which was assumed to be temperature-independent.

Density functional theory used no fitting parameters, even for the pure components, and is thus fully predictive once the PC-SAFT parameters are fixed.

4. Results

All calculations in this work have been done with the thermodynamic software Thermopack [31,54], complementing with CoolProp [71] and REFPROP 10 [32] for accurate reference EoS. Interfacial properties obtained from DFT have been computed using the SurfPack package [72]. The parameters fitted according to the procedure in Section 3 as well as the literature parameters are listed in the Supplementary Material.

The accuracy of an EoS for a property Y will be quantified with the mean absolute percentage deviation (MAPE) from the reference model. This is calculated as

$$\mathrm{MAPE}(Y) = \frac{100}{N} \times \sum_{k=1}^{N} \left| \frac{Y_k^{\mathrm{EoS}} - Y_k^{\mathrm{ref}}}{Y_k^{\mathrm{ref}}} \right|, \tag{31}$$

where $k = 1, \ldots, N$ indexes the state points used for evaluation.

4.1. Bulk properties of pure components

Table 2 summarizes the performance of the EoS after fitting their parameters for the pure components water and ammonia. As expected, the fitted models generally have lower deviations than the literature parameters, as the latter use different objective functions and possibly different reference databases. The best-performing generic EoS is for both fluids the PR EoS with linearly temperature-dependent volume shift, denoted PR-$c(T)$, which is also the one with the most tunable parameters. The PR EoS incorporates the exact critical temperature and pressure and reproduces saturation pressures accurately up to the critical temperature. All other EoS overestimate T_c and P_c. For ammonia, both CPA and PC-SAFT yield similar accuracy using either of the association schemes tested. We recommend the 2B scheme (one positive and one negative site) since it is the simplest.

The PR-$c(T)$ is particularly accurate for water. An accurate description of water is important to many systems [21,73]. We find that PR with a linear temperature dependence of the volume shift parameter (PR-$c(T)$ in Table 2) yields significant improvement in the accuracy for liquid densities and isochoric heat capacities (Table 2), at least up to 550 K, as shown in Fig. 1. A linear temperature dependence has no impact on the other properties in Table 2, as also argued by Jaubert et al. [50]. CPA also yields an excellent description of saturation properties, but unlike the cubic EoS, it significantly overestimates the critical temperature and pressure.

The physical validity of a temperature-dependent covolume has been questioned by Kalikhman et al. [51], who demonstrated that any repulsive term involving temperature-dependent covolumes results in a negative infinite value for the isochoric heat capacity at infinite pressure. In the supplementary material, we show the occurrence of negative isochoric heat capacity for water with a temperature-dependent volume shift. This has no practical consequences, as it only occurs at pressures above 1000 MPa, far outside the range of validity of the EoS. There are also no unphysical crossings of density isotherms near the critical point, which can occur if temperature-dependent volume shifts are carelessly implemented.

The quantity corresponding to molecular volume in a cubic EoS is the covolume, which effectively becomes $b-c(T)$ when applying volume shift. With the optimal parameters for $c(T)$ provided in the supplementary material, the effective covolume decreases with temperature. This coincides with how hydrogen-bonding influences the effective molecular volume: increasing temperature tends to break hydrogen bonds and pack the water molecules more densely. This may be why a temperature-dependent volume shift works so well for liquid water, but less so for other components.

Note however that a volume shift barely alters vapor phase properties and thus cannot capture the increase in heat capacities due to hydrogen bonding (cf. Fig. 1, right column). A volume shift is ultimately an empirical way to tune liquid-phase properties which, upon

Table 2
Mean absolute percentage deviations for the EoS for pure ammonia and pure water. Deviations were calculated for saturated vapor pressure, liquid density, latent heat, and isochoric and isobaric liquid heat capacity. Evaluation was done over an equispaced grid of 50 saturation temperatures between the triple point and $0.9T_c$ for ammonia, and 250 K and $0.8T_c$ for water. The parameters taken from literature were not fitted to minimize these exact deviations. The last three columns show percentage error in the critical temperature, pressure and density. All numbers in the table correspond to relative deviations, and are thus unitless.

EoS	p^{sat}	$\rho^{sat}(\ell)$	Δh^{sat}	$c_v^{sat}(\ell)$	$c_p^{sat}(\ell)$	T_c	P_c	ρ_c
Ammonia — fitted parameters								
CPA 2B	0.05	0.36	2.26	6.04	1.02	3.02	19.81	−7.05
PR	0.21	1.45	2.88	6.85	4.75	0.01	0.94	−16.62
PR-$c(T)$	0.25	1.23	2.87	3.69	5.05	0.01	0.94	−16.15
PC-SAFT 2B	0.15	0.10	1.76	5.83	1.91	3.32	21.37	−6.51
Ammonia — literature parameters								
SAFT-VR Mie 4C [44]	1.49	0.28	4.92	16.77	10.38	0.46	5.80	−3.82
PC-SAFT 2B [19]	2.22	0.50	8.83	8.05	21.15	2.19	16.41	−2.93
Water — fitted parameters								
PR-$c(T)$	0.05	0.47	1.08	1.31	2.51	0.03	−0.07	−18.59
PR	0.06	2.88	1.08	27.12	2.51	0.03	−0.07	−21.58
PC-SAFT 4C	0.08	1.29	2.17	15.08	5.33	10.62	89.02	10.18
CPA 4C	0.10	0.90	0.31	6.42	1.72	6.34	43.80	0.63
Water — literature parameters								
CPA 4C [59]	1.22	1.12	1.73	10.91	6.99	5.27	38.12	1.05
SAFT-VR Mie 4C [44]	1.39	0.68	1.82	19.48	4.60	4.94	35.59	1.90
PC-SAFT 4C [21]	2.03	0.81	1.95	16.18	13.89	6.90	63.60	3.63
PC-SAFT 2B [36]	2.88	6.99	2.43	22.26	17.70	7.77	65.97	2.94
PCP-SAFT 4C [21]	3.52	0.73	2.46	20.09	20.11	4.98	50.35	2.82
PC-SAFT 4C [75]	4.00	2.33	2.48	17.30	18.40	8.52	73.74	6.21
PC-SAFT 4C [19]	4.06	2.30	3.33	20.42	23.79	9.50	94.96	14.18
PC-SAFT 2B [21]	5.67	0.94	7.39	31.62	30.07	4.67	46.73	4.65
PCP-SAFT 3B [21]	11.30	0.68	5.18	43.31	41.12	2.13	35.18	1.90

Table 3
Mean absolute percentage deviations for mole fractions of binary models, where x and y correspond to the liquid and vapor phase compositions, respectively. The average is taken for temperatures 250 K, 273.15 K, 300 K, 350 K, 400 K, and 450 K.

Model	x (%)	y (%)
PR	3.9	6.1
CPA	5.4	8.1
PC-SAFT (DGT)	11.2	12.9
PC-SAFT (DFT)	8.5	19.8

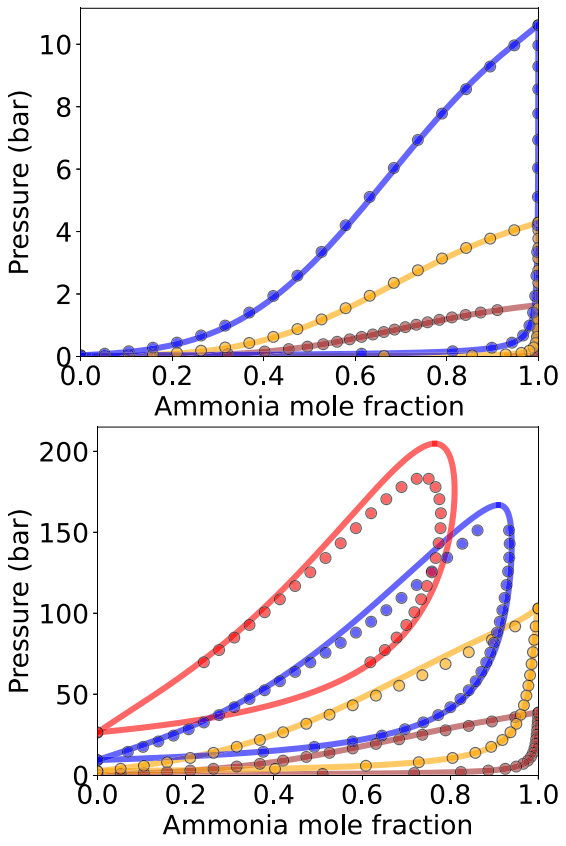

Fig. 2. Pxy phase diagrams for the ammonia–water mixture at 245 K, 273.15 K and 300 K (top) and 350 K, 400 K, 450 K and 500 K (bottom), calculated with PR-$c(T)$ (curves) and the reference model (markers).

introducing temperature-dependence, turns out to be particularly effective for liquid water. The optimal alpha parameters (L, M, N) listed in the supplementary material have been verified to be "consistent" in the sense of le Guennec et al. [74], meaning they are expected to extrapolate in a reasonable manner beyond their fitting range.

Table 2 shows that the heat capacity of water along the saturation curve is poorly represented by most other EoS than PR-$c(T)$. One reason for this may be that the literature parameters for CPA and PC-SAFT that we have found were fitted only to saturation pressures and liquid densities, with equal weight [16,19,21,36,59,75]. Although these properties are usually the most accurately known, such approaches run the risk of poorly reproducing caloric properties. Piña-Martinez et al. [76] analyzed the choice of objective function for tuning cubic EoS over a large database, and found that explicitly including isobaric heat capacity in the objective function was necessary to reproduce it properly. Table 2 in this work and Ref. [52] moreover illustrate that c_v should also be included, as even with low deviations in c_p, there can be large deviations in c_v.

4.2. Bulk properties of the ammonia–water mixture

The ammonia–water phase behavior only has vapor–liquid equilibrium, with no liquid–liquid equilibrium or azeotropes. It is a Type I mixture according to the taxonomy of van Konynenburg and Scott [77].

Fig. 2 shows that PR predicts accurately the compositions of coexisting vapor and liquid, although it overestimates the critical pressure somewhat at the highest temperatures. Fig. 3 shows the liquid mixture densities and the enthalpy of mixing, $h^{mix}(T, P, \boldsymbol{x}) = h(T, P, \boldsymbol{x}) - \sum_i x_i h_i^{pure}(T, P)$. The enthalpy of mixing has a qualitatively correct, exothermic behavior, but its magnitude is overestimated by roughly 20%.

Peng Robinson with the Huron–Vidal mixing rule, having two fitted parameters, yields more accurate results than the CPA or PC-SAFT models, each having one fitted parameter (see Table 3). Despite the difference in number of parameters, we have found that even if the latter two models are fitted at each temperature, they do not yield as high accuracy as PR. The reason may be that the Huron–Vidal mixing rule accounts for the possibility of each component experiencing a local composition different than the overall composition [78]. This local-composition effect can be prominent for systems with strong intermolecular forces such as the ammonia–water system. It stands in contrast to the random mixing approach implicit in the standard CPA and PC-SAFT mixing rules, where interaction energies are calculated by simple mole-fraction averaging such as Eq. (15). Applying local-composition mixing rules for SAFT-type EoS is straightforward for non-associating components [79], although more work is needed for associating components like ammonia and water.

The DGT model uses the PC-SAFT parameters fitted in this work (see supplementary material). The DFT model uses the same parameters for ammonia but the PC-SAFT 2B [21] water parameters optimized for DFT.

4.3. Interfacial properties

4.3.1. Density profiles

Density profiles for the ammonia–water mixtures at 293.15 K calculated from the PC-SAFT DGT and DFT are shown in Fig. 4. The

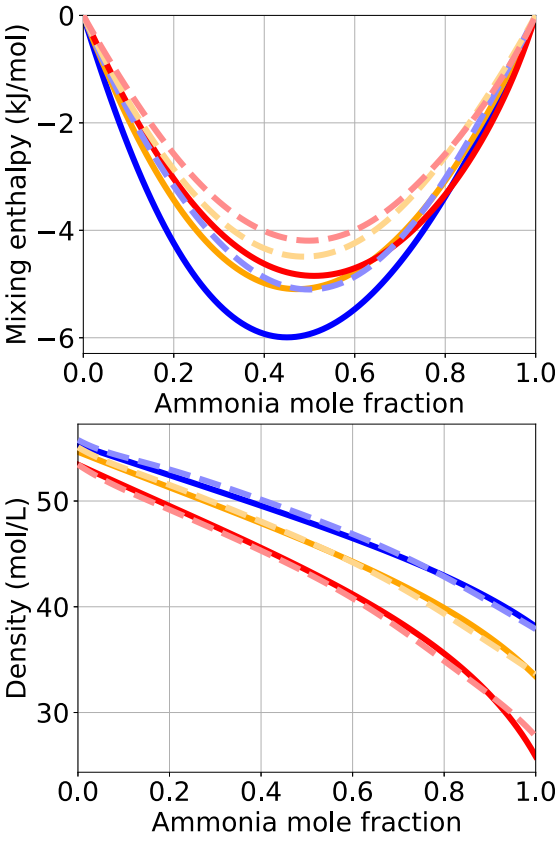

Fig. 3. Enthalpy of mixing (top) and mixture density (bottom) for the ammonia–water mixture at 100 bar. Three isotherms are shown: 273.15 K (blue), 323.15 (orange), 373.15 (red). Curves for the PR EoS (full lines) and the reference EoS (dashed lines) are shown. All states correspond to a liquid phase.

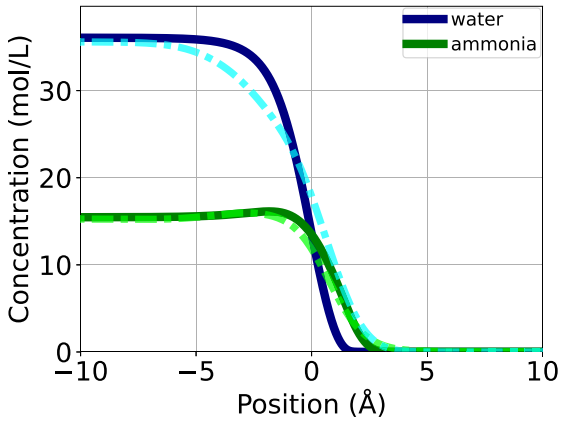

Fig. 4. Calculated density profiles of water (blue curves) and ammonia (green curves) through a planar vapor–liquid interface of the ammonia–water mixture at 293.15 K and a liquid ammonia mole fraction of $x_{NH_3} = 0.3$. The full curves correspond to PC-SAFT DGT with $\beta_{ij} = 0.3$, and dash–dot curves correspond to DFT.

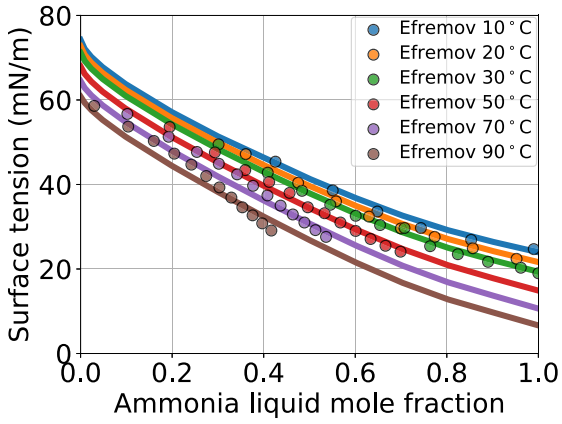

Fig. 5. Surface tension measurements by Efremov and Golubev [85] and the fitted PC-SAFT DGT model with $\beta_{ij} = 0.8$.

densities on each side asymptotically approach the bulk densities from the vapor–liquid equilibrium calculations of the EoS. Of particular interest is the maximum in the ammonia density profile in the interfacial region. The maximum suggests that there is an excess of ammonia molecules residing at the interface. Chandra et al. [80,81] investigated vapor–liquid interfaces of ammonia–water mixtures by use of molecular dynamics simulations, using force fields that model atoms as a Lennard-Jones site with a partial Coulomb charge. Their simulated ammonia concentrations across the interface profiles also had a peak of ammonia at the interface.

In addition to the maximum, another interesting feature of DGT's ammonia density profile is the small, local minimum on the liquid side of the maximum. Such a morphology has been observed in previous works using DGT [82,83], and was recently reviewed by Stephan et al. [84], who classified it as "Type iv" behavior. Consistent with previous findings [82,83], we have found that this minimum is a consequence of the geometric mixing rule for the influence parameters, i.e. $\kappa_{ij} = \sqrt{\kappa_i \kappa_j}$. The minimum disappears for $\beta_{ij} \geq 0.1$. DFT also exhibits Type iv behavior, albeit the minimum and the maximum are much less pronounced.

4.3.2. Surface tensions

Planar surface tension measurements in the open literature are scarce. The most comprehensive data set has been published by Efremov and Golubev [85]. Using a capillary rise technique, they performed measurements between 1 and 12 atm and between 293.15 K and 373.15 K. To achieve a decent performance with DGT, we had to tune the cross influence parameter for the mixture. Using $\beta_{ij} = 0.8$, the results in Fig. 5 are obtained. We observe that the fit is excellent at temperatures below 50 °C, but deteriorates at higher temperatures. We note that the capillary rise method makes use of the density of the vapor and liquid phases at the given temperature and pressure, which Efremov and Golubev found by correlating literature data. It is unclear how accurately this was accomplished in the 1960s. Especially for the highest temperatures, the available literature data could have been scarce, and their reported surface tensions are therefore likely to be less reliable in this regime.

The remaining surface tension measurements have been performed at ambient temperature. Two notable works in this regard are that of Rice [25] from 1928 at 291.65 K and that of King et al. [23] at 293.15 K. These surface tensions (cf. Fig. 6) are higher than those reported by Efremov and Golubev [85], by as much as 10% for some concentrations. However, the measurements by Rice and King et al. are highly consistent with each other. Donaldson [24] further showed that the measurements by Rice are consistent with his own measurements at 298.15 K, although it is unclear how the temperature conversion was carried out. As a final, qualitative argument for the correctness of the measurements of Rice and King et al. we note that they exhibit the same wavy shape when plotted against the ammonia liquid mole fraction (Fig. 6) as was observed in the molecular simulation study by Paul and Chandra [80].

4.3.3. Adsorptions

The planar adsorptions at 293.15 K from theory and experiments are shown in Fig. 7, calculated for the total equimolar surface. Ammonia is

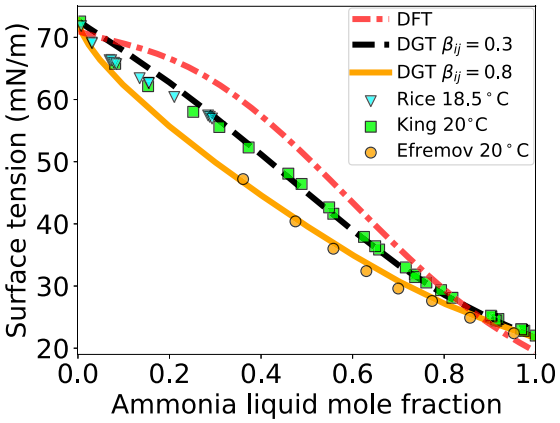

Fig. 6. Surface tension measurements at ~293.15 K by Rice [25] (blue triangles), King et al. [23] (green squares) and Efremov and Golubev [85] (orange dots). The curves correspond to the PC-SAFT DFT model (red dash–dot curve), PC-SAFT DGT model with $\beta_{ij} = 0.8$ (orange full curve), and $\beta_{ij} = 0.3$ (black dashed curve).

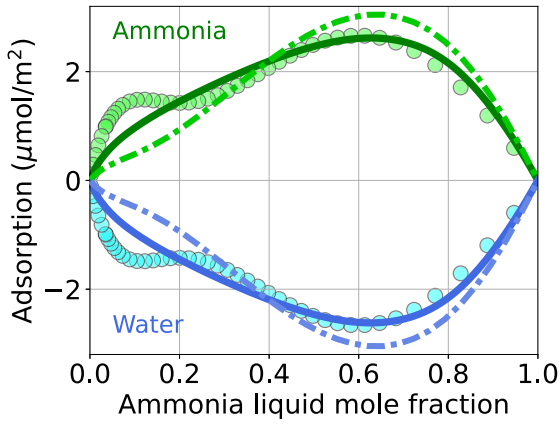

Fig. 7. Adsorptions of ammonia and water for planar interfaces at 293.15 K (20 °C) calculated with DGT and DFT. The full curves correspond to $\beta_{ij} = 0.3$ and the dash-dotted to DFT. The circles are inferred from the experimental data via the reference EoS. The adsorption was calculated relative to the total equimolar surface.

adsorbed at the interface, reaching a maximum of ~ 3 μmol/m^2. Experimental adsorptions were inferred from isothermal experimental surface tension data through Eq. (20), using the King correlation presented by Hyvärinen et al. [86] and the reference equation of state [32] as input.

The wavy shape of the surface tension data manifests as a plateau in the experimentally determined adsorptions, occurring for liquid ammonia mole fraction between 0.1 and 0.2. Donaldson [24] found a similar plateau from their measurements at 298.15 K. None of the models reproduce this feature, although for $x_{NH_3} > 0.4$ DFT yields a decent and DGT an excellent match.

5. Conclusion

Ammonia is a promising energy carrier for the green transition. However, the sensitivity of small concentrations for both safety and environmental applications place stringent demands on the accuracy of thermodynamic models.

In this work, we have investigated the bulk and interfacial thermodynamic properties of mixtures of ammonia and water, focusing on the Peng–Robinson (PR), cubic plus association (CPA), and PC-SAFT equations of state. The available literature provide several parameter sets for water, but only a few for ammonia. We refitted parameters to a range of saturation properties, where supercooled properties down to 250 K were included for water. For ammonia, all three EoS yield good results, with PR slightly outperforming the other two. For water, CPA is slightly more accurate than PC-SAFT, but the PR EoS with a temperature-dependent volume shift was found to be most accurate.

Given the widespread use of cubic EoS and the importance of water, the success of using a temperature-dependent volume shift for water is notable. For the liquid phase, it clearly outperforms all other EoS considered (except for the reference EoS). Comparing it to the PR EoS with constant volume shift, we see that the linear temperature dependence reduces errors from 2.9% to 0.5% for densities and from 27% to 1.3% for isochoric heat capacities, leaving the other properties essentially unchanged. We speculate that the success is because a temperature-dependent covolume mimics the strong influence of hydrogen-bonding on density. This explanation is consistent with the dependence of the volume shift on temperature, and the fact that it does not significantly improve the fit for ammonia.

For correlating vapor–liquid equilibrium (VLE) compositions, we found that PR with Huron–Vidal mixing rules yields relative deviations of 3.9% and 6.1% for vapor and liquid phase compositions, respectively. It outperforms CPA and PC-SAFT with their standard mixing rules. Given that CPA and PC-SAFT reproduce the pure-component properties well, the reason why they are outperformed lies in the mixing rule. More work on incorporating other mixing rules, e.g. based on the local-composition concept, may be beneficial. At present, cubic EoS with excess Gibbs mixing rules retains a prominent position as a simple, flexible, well-understood and accurate correlation tool among the common engineering-type EoS.

We reviewed the open literature on the interfacial thermodynamics of the ammonia–water system, and found that experimental data for surface tensions are lacking. In fact, there are high-quality, consistent data sets available only at 293.15 K — a surprising finding given the ubiquity of the ammonia–water system.

To model the vapor–liquid interface, we applied density gradient theory (DGT) and density functional theory (DFT), both based on PC-SAFT. DGT, having three tunable parameters yielded the best description of surface tensions and adsorptions. DFT, with no tunable parameters, still yielded a decent description — an impressive feat for a model only fitted to bulk thermodynamic properties. Neither model reproduced the qualitative behavior of the surface tension and adsorption of dilute aqueous ammonia solutions. This suggests that more work is needed to understand and describe the interfacial thermodynamics of the ammonia–water system both on the experimental and modeling side.

CRediT authorship contribution statement

Ailo Aasen: Writing – review & editing, Writing – original draft, Software, Methodology, Investigation, Formal analysis, Conceptualization. **Vegard G. Jervell:** Writing – review & editing, Writing – original draft, Validation, Software, Investigation. **Morten Hammer:** Writing – review & editing, Software, Methodology, Investigation, Formal analysis, Conceptualization. **Bjørn A. Strøm:** Writing – review & editing, Software, Investigation. **Hans L. Skarsvåg:** Writing – review & editing, Validation, Methodology. **Øivind Wilhelmsen:** Writing – review & editing, Supervision, Methodology, Conceptualization.

Declaration of competing interest

The authors declare that they have no known competing financial interests or personal relationships that could have appeared to influence the work reported in this paper.

Data availability

Data will be made available on request.

Acknowledgments

This work was funded by the Research Council of Norway through the MaritimeNH3 project, project number 328679. This work was partly supported by the Research Council of Norway through its Centres of Excellence funding scheme, Porelab, Project Number 262644.

Appendix A. Supplementary data

Supplementary material related to this article can be found online at https://doi.org/10.1016/j.fluid.2024.114125.

References

[1] K. Gao, J. Wu, I.H. Bell, A.H. Harvey, E.W. Lemmon, A reference equation of state with an associating term for the thermodynamic properties of ammonia, J. Phys. Chem. Ref. Data 52 (1) (2023).
[2] J. Hansson, S. Brynolf, E. Fridell, M. Lehtveer, The potential role of ammonia as marine fuel—based on energy systems modeling and multi-criteria decision analysis, Sustainability 12 (8) (2020) 3265, http://dx.doi.org/10.3390/su12083265.
[3] M.J. Fedoruk, R. Bronstein, B.D. Kerger, Ammonia exposure and hazard assessment for selected household cleaning product uses, J. Expo. Sci. Environ. Epidemiology 15 (6) (2005) 534–544, http://dx.doi.org/10.1038/sj.jea.7500431.
[4] Y. Liu, H.H. Ngo, W. Guo, L. Peng, D. Wang, B. Ni, The roles of free ammonia (FA) in biological wastewater treatment processes: A review, Environ. Int. 123 (2019) 10–19, http://dx.doi.org/10.1016/j.envint.2018.11.039.
[5] S. Ghavam, M. Vahdati, I. Wilson, P. Styring, Sustainable ammonia production processes, Front. Energy Res. 9 (2021) 34, http://dx.doi.org/10.3389/fenrg.2021.580808.
[6] A. Pearson, Refrigeration with ammonia, Int. J. Refrig. 31 (4) (2008) 545–551, http://dx.doi.org/10.1016/j.ijrefrig.2007.11.011.
[7] J.H. Seinfeld, S.N. Pandis, Atmospheric Chemistry and Physics: from Air Pollution to Climate Change, John Wiley & Sons, 2016.
[8] A. Valera-Medina, H. Xiao, M. Owen-Jones, W.I. David, P. Bowen, Ammonia for power, Prog. Energy Combust. Sci. 69 (2018) 63–102, http://dx.doi.org/10.1016/j.pecs.2018.07.001.
[9] A. Valera-Medina, F. Amer-Hatem, A.K. Azad, I.C. Dedoussi, M. de Joannon, R.X. Fernandes, P. Glarborg, H. Hashemi, X. He, S. Mashruk, J. McGowan, C. Mounaim-Rouselle, A. Ortiz-Prado, A. Ortiz-Valera, I. Rossetti, B. Shu, M. Yehia, H. Xiao, M. Costa, Review on ammonia as a potential fuel: From synthesis to economics, Energy Fuels (ISSN: 1520-5029) 35 (9) (2021) 6964–7029, http://dx.doi.org/10.1021/acs.energyfuels.0c03685.
[10] R.P. Padappayil, J. Borger, Ammonia toxicity, in: StatPearls [Internet], StatPearls Publishing, 2023.
[11] D.J. Randall, T. Tsui, Ammonia toxicity in fish, Mar. Pollut. Bull. 45 (1–12) (2002) 17–23, http://dx.doi.org/10.1016/S0025-326X(02)00227-8.
[12] M.S. Wertheim, Fluids with highly directional attractive forces. I. Statistical thermodynamics, J. Stat. Phys. 35 (1) (1984) 19–34, http://dx.doi.org/10.1007/BF01017362.
[13] M.S. Wertheim, Fluids with highly directional attractive forces. II. Thermodynamic perturbation theory and integral equations, J. Stat. Phys. 35 (1) (1984) 35–47, http://dx.doi.org/10.1007/BF01017363.
[14] M.S. Wertheim, Fluids with highly directional attractive forces. III. Multiple attraction sites, J. Stat. Phys. 42 (3) (1986) 459–476, http://dx.doi.org/10.1007/BF01127721.
[15] M.S. Wertheim, Fluids with highly directional attractive forces. IV. Equilibrium polymerization, J. Stat. Phys. 42 (3) (1986) 477–492, http://dx.doi.org/10.1007/BF01127722.
[16] L. Grandjean, J.-C. de Hemptinne, R. Lugo, Application of GC-PPC-SAFT EoS to ammonia and its mixtures, Fluid Phase Equilib. 367 (2014) 159–172, http://dx.doi.org/10.1016/j.fluid.2014.01.025.
[17] N. Mac Dowell, F.E. Pereira, F. Llovell, F. Blas, C.S. Adjiman, G. Jackson, A. Galindo, Transferable SAFT-VR models for the calculation of the fluid phase equilibria in reactive mixtures of carbon dioxide, water, and n-alkylamines in the context of carbon capture, J. Phys. Chem. B 115 (25) (2011) 8155–8168, http://dx.doi.org/10.1021/jp107467s.
[18] I. Polishuk, J.M. Garrido, Comparison of SAFT-VR-mie and CP-PC-SAFT in predicting phase behavior of associating systems I. Ammonia–water, methanol, ethanol and hydrazine, J. Mol. Liq. 265 (2018) 639–653, http://dx.doi.org/10.1016/j.molliq.2018.05.112.
[19] D. NguyenHuynh, C.T. Mai, S.T. Tran, X.T. Nguyen, O. Baudouin, Modelling of phase behavior of ammonia and its mixtures using the mg-SAFT, Fluid Phase Equilib. 523 (2020) 112689, http://dx.doi.org/10.1016/j.fluid.2020.112689.
[20] J. Gross, J. Vrabec, An equation-of-state contribution for polar components: dipolar molecules, AIChE J. 52 (3) (2006) 1194–1204, http://dx.doi.org/10.1002/aic.10683.
[21] P. Rehner, J. Gross, Multiobjective optimization of PCP-SAFT parameters for water and alcohols using surface tension data, J. Chem. Eng. Data 65 (12) (2020) 5698–5707, http://dx.doi.org/10.1021/acs.jced.0c00684.
[22] X. Xu, S. Lasala, R. Privat, J.-N. Jaubert, E-PPR78: A proper cubic EoS for modelling fluids involved in the design and operation of carbon dioxide capture and storage (CCS) processes, Int. J. Greenh. Gas Control 56 (2017) 126–154, http://dx.doi.org/10.1016/j.ijggc.2016.11.015.
[23] H. King, J.L. Hall, G.C. Ware, A study of the density, surface tension and adsorption in the water-ammonia system at 20 C, J. Am. Chem. Soc. 52 (12) (1930) 5128–5135, http://dx.doi.org/10.1021/ja01375a073.
[24] D. Donaldson, Adsorption of atmospheric gases at the air-water interface. I. NH3, J. Phys. Chem. A 103 (1) (1999) 62–70, http://dx.doi.org/10.1021/jp9833247.
[25] O.K. Rice, The surface tension and the structure of the surface of aqueous ammonia solutions., J. Phys. Chem. 32 (4) (1928) 583–592, http://dx.doi.org/10.1021/j150286a009.
[26] A. Aasen, D. Reguera, Ø. Wilhelmsen, Curvature corrections remove the inconsistencies of binary classical nucleation theory, Phys. Rev. Lett. 124 (2020) 045701, http://dx.doi.org/10.1103/PhysRevLett.124.045701.
[27] A. Aasen, E.M. Blokhuis, Ø. Wilhelmsen, Tolman lengths and rigidity constants of multicomponent fluids: Fundamental theory and numerical examples, J. Chem. Phys. 148 (20) (2018) 204702, http://dx.doi.org/10.1063/1.5026747.
[28] P. Rehner, A. Aasen, Ø. Wilhelmsen, Tolman lengths and rigidity constants from free-energy functionals–General expressions and comparison of theories, J. Chem. Phys. 151 (24) (2019) 244710, http://dx.doi.org/10.1063/1.5135288.
[29] P. Rehner, J. Gross, Surface tension of droplets and Tolman lengths of real substances and mixtures from density functional theory, J. Chem. Phys. 148 (16) (2018) 164703, http://dx.doi.org/10.1063/1.5020421.
[30] M. Hammer, G. Bauer, R. Stierle, J. Gross, Ø. Wilhelmsen, Classical density functional theory for interfacial properties of hydrogen, helium, deuterium, neon, and their mixtures, J. Chem. Phys. 158 (10) (2023) http://dx.doi.org/10.1063/5.0137226.
[31] Ø. Wilhelmsen, A. Aasen, G. Skaugen, P. Aursand, A. Austegard, E. Aursand, M.A. Gjennestad, H. Lund, G. Linga, M. Hammer, Thermodynamic modeling with equations of state: Present challenges with established methods, Ind. Eng. Chem. Res. 56 (13) (2017) 3503–3515, http://dx.doi.org/10.1021/acs.iecr.7b00317.
[32] E.W. Lemmon, I.H. Bell, M. Huber, M. McLinden, NIST standard reference database 23: reference fluid thermodynamic and transport properties-REFPROP, version 10.0, Standard Reference Data Program, Gaithersburg, 2018.
[33] R. Tillner-Roth, D.G. Friend, A Helmholtz free energy formulation of the thermodynamic properties of the mixture {water+ammonia}, J. Phys. Chem. Ref. Data 27 (1) (1998) 63–96, http://dx.doi.org/10.1063/1.556015.
[34] C. Cheng, W. Tan, L. Liu, Numerical simulation of water curtain application for ammonia release dispersion, J. Loss Prev. Process. Ind. 30 (2014) 105–112, http://dx.doi.org/10.1016/j.jlp.2014.05.003.
[35] J. Gross, G. Sadowski, Perturbed-chain SAFT: An equation of state based on a perturbation theory for chain molecules, Ind. Eng. Chem. Res. 40 (4) (2001) 1244–1260, http://dx.doi.org/10.1021/ie0003887.
[36] J. Gross, G. Sadowski, Application of the perturbed-chain SAFT equation of state to associating systems, Ind. Eng. Chem. Res. 41 (22) (2002) 5510–5515, http://dx.doi.org/10.1021/ie010954d.
[37] J. Gross, A density functional theory for vapor-liquid interfaces using the PCP-SAFT equation of state, J. Chem. Phys. 131 (2009) 204705, http://dx.doi.org/10.1063/1.3263124.
[38] P. Rehner, J. Gross, Predictive density gradient theory based on nonlocal density functional theory, Phys. Rev. E 98 (6) (2018) 063312, http://dx.doi.org/10.1103/physreve.98.063312.
[39] T. Boublík, Hard-sphere equation of state, J. Chem. Phys. 53 (1) (1970) 471–472, http://dx.doi.org/10.1063/1.1673824.
[40] G.A. Mansoori, N.F. Carnahan, K.E. Starling, T.W. Leland Jr., Equilibrium thermodynamic properties of the mixture of hard spheres, J. Chem. Phys. 54 (4) (1971) 1523–1525, http://dx.doi.org/10.1063/1.1675048.
[41] S.H. Huang, M. Radosz, Equation of state for small, large, polydisperse, and associating molecules, Ind. Eng. Chem. Res. 29 (11) (1990) 2284–2294, http://dx.doi.org/10.1021/ie00107a014.
[42] W.G. Chapman, K.E. Gubbins, G. Jackson, M. Radosz, New reference equation of state for associating liquids, Ind. Eng. Chem. Res. 29 (8) (1990) 1709–1721, http://dx.doi.org/10.1021/ie00104a021.
[43] T. Lafitte, A. Apostolakou, C. Avendaño, A. Galindo, C.S. Adjiman, E.A. Müller, G. Jackson, Accurate statistical associating fluid theory for chain molecules formed from Mie segments, J. Chem. Phys. 139 (15) (2013) 154504, http://dx.doi.org/10.1063/1.4819786.
[44] S. Dufal, T. Lafitte, A.J. Haslam, A. Galindo, G.N. Clark, C. Vega, G. Jackson, The A in SAFT: developing the contribution of association to the Helmholtz free energy within a Wertheim TPT1 treatment of generic Mie fluids, Mol. Phys. 113 (9–10) (2015) 948–984, http://dx.doi.org/10.1080/00268976.2015.1029027.
[45] D.Y. Peng, D.B. Robinson, A New Two-Constant Equation of State, Ind. Eng. Chem. Fund. 15 (1976) 59, http://dx.doi.org/10.1021/i160057a011.

[46] Y. Le Guennec, R. Privat, J.-N. Jaubert, Development of the translated-consistent tc-PR and tc-RK cubic equations of state for a safe and accurate prediction of volumetric, energetic and saturation properties of pure compounds in the sub-and super-critical domains, Fluid Phase Equilib. 429 (2016) 301–312, http://dx.doi.org/10.1016/j.fluid.2016.09.003.

[47] C.H. Twu, D. Bluck, J.R. Cunningham, J.E. Coon, A cubic equation of state with a new alpha function and a new mixing rule, Fluid Phase Equilib. 69 (1991) 33–50, http://dx.doi.org/10.1016/0378-3812(91)90024-2.

[48] M.-J. Huron, J. Vidal, New mixing rules in simple equations of state for representing vapour-liquid equilibria of strongly non-ideal mixtures, Fluid Phase Equilib. 3 (4) (1979) 255–271, http://dx.doi.org/10.1016/0378-3812(79)80001-1.

[49] A. Péneloux, E. Rauzy, R. Fréze, A consistent correction for Redlich–Kwong–Soave volumes, Fluid Phase Equilib. 8 (1) (1982) 7–23, http://dx.doi.org/10.1016/0378-3812(82)80002-2.

[50] J.-N. Jaubert, R. Privat, Y. Le Guennec, L. Coniglio, Note on the properties altered by application of a Péneloux–type volume translation to an equation of state, Fluid Phase Equilib. 419 (2016) 88–95, http://dx.doi.org/10.1016/j.fluid.2016.03.012.

[51] V. Kalikhman, D. Kost, I. Polishuk, About the physical validity of attaching the repulsive terms of analytical EOS models by temperature dependencies, Fluid Phase Equilib. 293 (2) (2010) 164–167, http://dx.doi.org/10.1016/j.fluid.2010.03.003.

[52] A. Aasen, M. Hammer, S. Lasala, J.-N. Jaubert, Ø. Wilhelmsen, Accurate quantum-corrected cubic equations of state for helium, neon, hydrogen, deuterium and their mixtures, Fluid Phase Equilib. 524 (2020) 112790, http://dx.doi.org/10.1016/j.fluid.2020.112790.

[53] R. Privat, J.-N. Jaubert, Y. Le Guennec, Incorporation of a volume translation in an equation of state for fluid mixtures: which combining rule? which effect on properties of mixing? Fluid Phase Equilib. 427 (2016) 414–420, http://dx.doi.org/10.1016/j.fluid.2016.07.035.

[54] SINTEF Energy Research/NTNU Department of Chemistry, ThermoTools: ThermoPack open source thermodynamics library, 2024, https://github.com/thermotools/thermopack.

[55] W. Wagner, A. Pruß, The IAPWS formulation 1995 for the thermodynamic properties of ordinary water substance for general and scientific use, J. Phys. Chem. Ref. Data 31 (2002) 387, http://dx.doi.org/10.1063/1.1461829.

[56] G.M. Kontogeorgis, E.C. Voutsas, I.V. Yakoumis, D.P. Tassios, An equation of state for associating fluids, Ind. Eng. Chem. Res. 35 (11) (1996) 4310–4318, http://dx.doi.org/10.1021/ie9600203.

[57] G. Soave, Equilibrium constants from a modified Redlich-Kwong equation of state, Chem. Eng. Sci. 27 (6) (1972) 1197–1203, http://dx.doi.org/10.1016/0009-2509(72)80096-4.

[58] G.M. Kontogeorgis, I.V. Yakoumis, H. Meijer, E. Hendriks, T. Moorwood, Multicomponent phase equlibrium calculations for water-methanol-alkane mixtures, Fluid Phase Equilib. 158–160 (1999) http://dx.doi.org/10.1016/S0378-3812(99)00060-6.

[59] G.M. Kontogeorgis, I.V. Yakoumis, H. Meijer, E. Hendriks, T. Moorwood, Multicomponent phase equilibrium calculations for water–methanol–alkane mixtures, Fluid Phase Equilib. 158 (1999) 201–209, http://dx.doi.org/10.1016/S0378-3812(99)00060-6.

[60] J. Rowlinson, B. Widom, Molecular Theory of Capillarity, Clarendon Press, Oxford, 1984.

[61] E. Sauer, J. Gross, Classical density functional theory for liquid–fluid interfaces and confined systems: A functional for the perturbed-chain polar statistical associating fluid theory equation of state, Ind. Eng. Chem. Res. 56 (14) (2017) 4119–4135, http://dx.doi.org/10.1021/acs.iecr.6b04551.

[62] R. Roth, Introduction to Density Functional Theory of Classical Systems: Theory and Applications, in: Lecture Notes, 2006.

[63] R. Stierle, E. Sauer, J. Eller, M. Theiss, P. Rehner, P. Ackermann, J. Gross, Guide to efficient solution of PC-SAFT classical density functional theory in various coordinate systems using fast Fourier and similar transforms, Fluid Phase Equilib. 502 (2020) http://dx.doi.org/10.1016/j.fluid.2019.112306.

[64] R.R. R. Evans, G. Kahl, New developments in classical density functional theory, J. Phys.: Condens. Matter. 28 (2016) http://dx.doi.org/10.1088/0953-8984/28/24/240401.

[65] P. Rehner, Interfacial Properties Using Classical Density Functional Theory: Curved Interfaces and Surfactants (Ph.D. thesis), University of Stuttgart, 2021.

[66] P. Tarazona, Free-energy density functional for hard spheres, Phys. Rev. A 31 (1985) 2672–2679, http://dx.doi.org/10.1103/PhysRevA.31.2672.

[67] Y.-X. Yu, J. Wu, A fundamental-measure theory for inhomogeneous associating fluids, J. Chem. Phys. 116 (16) (2002) 7094–7103, http://dx.doi.org/10.1063/1.1463435.

[68] J.S. Rowlinson, Translation of J. D. van der Waals' "The thermodynamic theory of capillarity under the hypothesis of a continuous variation of density", J. Stat. Phys. 20 (2) (1979) 197–200, http://dx.doi.org/10.1007/BF01011513.

[69] V. Holten, J.V. Sengers, M.A. Anisimov, Equation of State for Supercooled Water at Pressures up to 400 MPa, J. Phys. Chem. Ref. Data 43 (2014) 043101, http://dx.doi.org/10.1063/1.4895593.

[70] A. Mulero, I. Cachadiña, M. Parra, Recommended correlations for the surface tension of common fluids, J. Phys. Chem. Ref. Data 41 (4) (2012) 043105, http://dx.doi.org/10.1063/1.4768782.

[71] I.H. Bell, J. Wronski, S. Quoilin, V. Lemort, Pure and Pseudo-pure Fluid Thermophysical Property Evaluation and the Open-Source Thermophysical Property Library CoolProp, Ind. Eng. Chem. Res. 53 (6) (2014) 2498–2508, http://dx.doi.org/10.1021/ie4033999.

[72] NTNU Department of Chemistry, ThermoTools: SurfPack open source surface- and interfacial properties, 2024, https://github.com/thermotools/SurfPack.

[73] A. Aasen, M. Hammer, G. Skaugen, J.P. Jakobsen, Ø. Wilhelmsen, Thermodynamic models to accurately describe the $PVTxy$-behavior of water/carbon dioxide mixtures, Fluid Phase Equilib. 442 (2017) 125–139, http://dx.doi.org/10.1016/j.fluid.2017.02.006.

[74] Y. Le Guennec, S. Lasala, R. Privat, J.-N. Jaubert, A consistency test for α-functions of cubic equations of state, Fluid Phase Equilib. 427 (2016) 513–538, http://dx.doi.org/10.1016/j.fluid.2016.07.026.

[75] A. Grenner, J. Schmelzer, N. von Solms, G.M. Kontogeorgis, Comparison of two association models (Elliott- Suresh- Donohue and simplified PC-SAFT) for complex phase equilibria of hydrocarbon- water and amine-containing mixtures, Ind. Eng. Chem. Res. 45 (24) (2006) 8170–8179, http://dx.doi.org/10.1021/ie0605332.

[76] A. Pina-Martinez, Y. Le Guennec, R. Privat, J.-N. Jaubert, P.M. Mathias, Analysis of the combinations of property data that are suitable for a safe estimation of consistent twu α-function parameters: Updated parameter values for the translated-consistent tc-PR and tc-RK cubic equations of state, J. Chem. Eng. Data 63 (10) (2018) 3980–3988, http://dx.doi.org/10.1021/acs.jced.8b00640.

[77] P.H.v. Konynenburg, R.L. Scott, Critical lines and phase equilibria in binary van der Waals mixtures, Philos. Trans. R. Soc. Lond. Ser. A 298 (1980) 495–540, http://dx.doi.org/10.1098/rsta.1980.0266.

[78] G.M. Kontogeorgis, G. Folas, Thermodynamic Models for Industrial Applications, Wiley, 2010, http://dx.doi.org/10.1002/9780470747537.

[79] P.J. Walker, Toward advanced, predictive mixing rules in SAFT equations of state, Ind. Eng. Chem. Res. 61 (49) (2022) 18165–18175, http://dx.doi.org/10.1021/acs.iecr.2c03464.

[80] S. Paul, A. Chandra, Liquid-vapor interfacial properties of water-ammonia mixtures: Dependence on ammonia concentration, J. Chem. Phys. 123 (17) (2005) http://dx.doi.org/10.1063/1.2107428.

[81] D. Chakraborty, A. Chandra, Hydrogen bonded structure and dynamics of liquid-vapor interface of water-ammonia mixture: An ab initio molecular dynamics study, J. Chem. Phys. 135 (11) (2011) http://dx.doi.org/10.1063/1.3637499.

[82] P. Cornelisse, The Gradient Theory Applied - Simultaneous Modelling of Interfacial Tension and Phase Behaviour (Ph.D. thesis), Delft University of Technology, 1997.

[83] J. Mairhofer, J. Gross, Modeling properties of the one-dimensional vapor-liquid interface: Application of classical density functional and density gradient theory, Fluid Phase Equilib. 458 (2018) 243–252, http://dx.doi.org/10.1016/j.fluid.2017.11.032.

[84] S. Stephan, H. Cárdenas, A. Mejía, E.A. Müller, The monotonicity behavior of density profiles at vapor-liquid interfaces of mixtures, Fluid Phase Equilib. 564 (2023) 113596, http://dx.doi.org/10.1016/j.fluid.2022.113596.

[85] Y. Efremov, I. Golubev, Surface tension of aqueous ammonia solutions, Russ. J. Phys. Chem. 36 (5) (1962).

[86] A.-P. Hyvärinen, T. Raatikainen, A. Laaksonen, Y. Viisanen, H. Lihavainen, Surface tensions and densities of H2SO4+NH3+water solutions, Geophys. Res. Lett. 32 (16) (2005) http://dx.doi.org/10.1029/2005GL023268.